

Lithium and Beryllium in the Gaia-Enceladus Galaxy

P. Molaro,^{1,3}[★] G. Cescutti,¹ and X. Fu²

¹ *INAF, Osservatorio Astronomico di Trieste, Via G.B. Tiepolo 11, I-34143 Trieste, Italy*

² *The Kavli Institute for Astronomy and Astrophysics at Peking University, Beijing 100871, China*

³ *IFPU, Istitute for the Fundamental Physics of the Universe, Via Beirut, 2, 34151, Grignano, Trieste, Italy*

Accepted XXX. Received YYY; in original form ZZZ

ABSTRACT

Data from Gaia DR2 and APOGEE surveys revealed a relatively new component in the inner Galactic halo, which is likely the dynamical remnant of a disrupted dwarf galaxy named Gaia-Enceladus that collided with the Milky Way about 10 Gyrs ago. This merging event offers an extraordinary opportunity to study chemical abundances of elements in a dwarf galaxy, since they are generally hampered in external galaxies. Here, we focus on ⁷Li and ⁹Be in dwarf stars which are out of reach even in Local Group galaxies. Searching in GALAH, Gaia-ESO survey and in literature, we found several existing ⁷Li abundance determinations of stars belonging to the Gaia-Enceladus galaxy. The ⁷Li abundances of stars at the low metallicity end overlap with those of the Galactic halo. These are effective extragalactic ⁷Li measurements, which suggest that the ⁷Li *Spite plateau* is universal, as is the cosmological ⁷Li problem. We found a ⁷Li-rich giant out of 101 stars, which suggests a small percentage similar to that of the Milky Way. We also collect ⁹Be abundance for a subsample of 25 Gaia-Enceladus stars from literature. Their abundances share the Galactic [Be/H] values at the low metallicity end but grow slower with [Fe/H] and show a reduced dispersion. This suggests that the scatter observed in the Milky Way could reflect the different ⁹Be evolution patterns of different stellar components which are mixed-up in the Galactic halo.

Key words: stars: abundances; Galaxy: stellar content – halo; galaxies: Enceladus – abundances; cosmology: Primordial nucleosynthesis.

1 INTRODUCTION

In the last decades kinematical and chemical surveys of the stars of the Galactic Halo revealed streams and structures belonging to different stellar groups (Nidever et al. 2012; Gaia Collaboration et al. 2016). One of the most studied is Sagittarius dSph, (Ibata et al. 2001). The stellar component of the Galactic halo showing low- $[\alpha/\text{Fe}]$ probably was also accreted from local dwarf galaxies (Gratton et al. 2003; Brook et al. 2003; Nissen & Schuster 2010; Kirby et al. 2009; Tolstoy et al. 2009). More recently, the ground based spectrographic survey APOGEE together with the astrometric results from the Gaia satellite DR2 revealed a component in the inner halo which shows a distinctive motion and metallicities $Z \approx Z_{\odot}/10$ which are relatively more metal-rich than the Galactic halo (Helmi et al. 2018; Haywood et al. 2018; Belokurov et al. 2018). This new structure, called Gaia-Enceladus or Gaia Sausage, likely represents a disrupted dwarf galaxy after collision with the Milky Way about 10 Gyr ago.

The stellar remnants of this merging offer unique opportunities to study in detail the abundances of the elements in a dwarf galaxy, normally hampered by their large distance. A detailed chemical analysis of the most studied elements in these stars has been already performed in (Vincenzo et al. 2019). Here, we focus on the elements ⁷Li and ⁹Be which have special nucleosynthetic origin and about which nothing or very little is known in extragalactic environments.

The nucleosynthetic origin of the light elements Li, Be and B differs from that of the other chemical elements. As was first recognized by Burbidge et al. (1957) they cannot be made in the stellar interior or in the explosive phases. They suggested an *X-mechanism* likely connected to spallation processes taking place onto the surfaces of magnetic stars or somewhat in the supernovae blow out. In fact, Li undergoes multiple nucleosynthetic processes. Wagoner et al. (1967) have shown that ⁷Li is made in the primordial nucleosynthesis and Reeves et al. (1970) suggested a cosmic-ray spallation occurring in the interstellar medium. The Li/H abundance measurements in the old Galactic halo stars are a factor of 3.5 lower than primordial nucleosynthesis predictions (Fields et al. 2014) and it is not clear whether this

[★] E-mail: paolo.molaro@inaf.it

mismatch comes from uncertainties in stellar astrophysics or nuclear inputs, or whether there is new physics at work, see [Fields \(2011\)](#) and references therein. Cross sections of BBN reactions are constrained by extensive laboratory measurements therefore making nuclear fix increasingly unlikely. Another possibility is a ${}^7\text{Li}$ destruction over the long stellar lifetimes by mechanisms such as microscopic diffusion ([Korn et al. 2006](#)), rotational mixing ([Pinsonneault et al. 1998](#)), or pre-main-sequence depletion ([Fu et al. 2015](#)). However, fine tuning of the initial stellar parameters is required to reduce lithium to the observed levels. On the other hand, one or more Galactic Li sources are needed to increase the Li abundance from the primordial value to that presently observed either in meteorites or in young stars of the Galaxy. Quite recently, novae have gained favour as the probable main Galactic sources with detection of ${}^7\text{Be}$ which later decays into ${}^7\text{Li}$ in their outbursts ([Tajitsu et al. 2015](#); [Molaro et al. 2016](#); [Izzo et al. 2018a,b](#); [Cescutti & Molaro 2019](#)). ${}^9\text{Be}$ is the only long-lived isotope of beryllium and is a pure product of cosmic-ray spallation ([Reeves et al. 1970](#)). Early theoretical models of the Galaxy predicted a secondary behaviour with a quadratic dependence on metallicity. However, early measurements of Be and B in metal-poor stars revealed a linear relation with metallicity which is characteristic of a primary production ([Rebolo et al. 1988](#); [Duncan et al. 1992](#)). [Duncan et al. \(1992\)](#) suggested that the principal channel of synthesis involves the collision of cosmic-ray CNO nuclei from the supernovae with interstellar protons as was already envisaged by [Burbidge et al. \(1957\)](#). Being a primary element, ${}^9\text{Be}$ abundance should trace the chemical evolution of other primary elements belonging Galactic component. In this paper we carefully search for extant ${}^7\text{Li}$ and ${}^9\text{Be}$ abundances of stars belonging to Gaia-Enceladus and we seek signatures of a different chemical evolution by comparing them to those of the Galaxy.

2 LITHIUM ABUNDANCES IN GAIA-ENCELADUS

[Helmi et al. \(2018\)](#) provided a sample of 4644 suggested Gaia-Enceladus member stars, a subsample of which are in the catalogue of The Apache Point Observatory Galactic Evolution Experiment (APOGEE) with determined abundances for 18 elements ([Nidever et al. 2012](#)). The Gaia-Enceladus subsample with APOGEE measurements includes stars with $[\alpha/\text{Fe}]$ values lower than that of the Milky Way halo stars in the metallicity range $-1.5 < [\text{Fe}/\text{H}] < -0.5$, which are typical of dwarf spheroidal galaxies and are also observed in the Damped Lyman- α galaxies [Rafelski et al. \(2012\)](#). APOGEE does not provide ${}^7\text{Li}$ abundances. Thus, we searched for the Gaia-Enceladus component in the GALAH DR2 survey ([Buder et al. 2018](#)), the Gaia-ESO DR3 survey ([Gilmore et al. 2012](#)) and in the literature by cross matching the larger sample of Gaia-Enceladus stars provided by [Helmi et al. \(2018\)](#) by considering their selection criteria, namely a distance of < 5 kpc and $L_z < 150$.

The cross-match between Gaia-Enceladus candidates with the GALAH yielded 121 stars which are provided in the online Table. The selection has been restricted to GALAH stars with $\text{flag}=0$ for the stellar parameters. 11 stars out of this sample have $[\text{Fe}/\text{H}] < -0.8$, $T_{\text{eff}} > 5700$ K and $\text{Logg} >$

3.65. The cuts have been chosen to avoid the stars in which Li has been depleted or diluted by main sequence or post main-sequence evolution. The Gaia-ESO survey provided only one giant star. By cross matching with the literature databases of JINA ([Abohalima & Frebel 2018](#)), SAGA ([Suda et al. 2008](#)) and [Aguilera-Gómez et al. \(2018\)](#) we found 31 additional Gaia-Enceladus dwarf star candidates that match the same criteria with extant lithium abundances¹. All 43 Gaia-Enceladus candidates are listed in Table 2. The kinematical properties of the selected Gaia-Enceladus candidates are reported in Table 2.

The energy (E_n) and the angular momentum in the Z direction (L_z) are adopted from [Helmi et al. \(2018\)](#). In addition, we have also computed the orbital parameters, including the apocenter distance (r_{apo}), the pericenter distance (r_{peri}), the maximum distance from the Galactic plane (Z_{max}) and eccentricity (ecc), based on the stellar orbit in the last 1 Gyr. For this calculation we use the public licensed code GALPOT following the method described in [McMillan \(2017\)](#), and assume a Galactic potential which includes thin and thick stellar disks, bulge, halo, and a gas disk. To note that almost all selected Gaia-Enceladus stars show high, almost parabolic eccentricity, which is different from the normal halo stars with a more circular orbit. This further supports the hypothesis that they are accreted. In the selection for Gaia-Enceladus candidates there is a strong probability of contaminations by thick disk stars in particular at relatively high metallicity. For instance, G 5-40 satisfies the kinematical cuts but shows a too high $[\alpha/\text{Fe}]$ ratio for a Gaia-Enceladus member ([Nissen & Schuster 2010](#)). In the following, we provide an analysis both with and without this star.

The $A(\text{Li})$ abundances vs. $[\text{Fe}/\text{H}]$ of the selected stars are shown in Figure 1. From the figure it can be seen that the Gaia-Enceladus stars show a very similar behavior to stars in the Milky Way in particular at low metallicity. The mean value of the 17 stars with $[\text{Fe}/\text{H}] < 2.0$ in Table 2 is $A(\text{Li}) = 2.18 \pm 0.10$ to be compared with the $A(\text{Li}) = 2.199 \pm 0.086$ found by [Sbordone et al. \(2010\)](#) in a similar metallicity range. However, there are three stars which present an enhancement of lithium at $[\text{Fe}/\text{H}] \approx -1$ which suggests a slightly different Li evolution in this dwarf galaxy. If novae are the main source which drive the Li enrichment in the Galaxy in a dwarf galaxy which is characterised by a slower star formation rate, their effects should start to be evident at lower metallicity. To sketch the evolution of Li in Gaia-Enceladus, we show in Figure 1 the thin disk evolution (thin line) and the same results with an offset of -0.5 dex in metallicity; the offset is applied to mimic the typical lower efficiency in a satellite galaxy ([Matteucci & Brocato 1990](#)). A possible model for the Li evolution in the Gaia-Enceladus galaxy has been also discussed in [Cescutti et al. \(2020\)](#).

3 LI-RICH GIANTS IN GAIA-ENCELADUS

When a star evolves off the main sequence, the surface convective zone deepens and material from the hotter interior is dredged up to the surface. Since ${}^7\text{Li}$ is a fragile element

¹ $A(\text{Li}) = \log \frac{n(\text{Li})}{n(\text{H})} + 12$

Table 1. Gaia-Enceladus candidate stars with Li and Be abundances measured from literature with $\log(g) > 3.65$ and $T_{eff} > 5700$ K. References for the stellar parameters and Li abundance are reported in the last column (first number) and those for Be in the second number: 1 (Buder et al. 2018), 2 Fulbright (2000), 3 Boesgaard & Novicki (2006), 4 Boesgaard et al. (2005), 5 Smiljanic et al. (2009), 6 Charbonnel & Primas (2005), 7 Asplund et al. (2006), 8 Spite et al. (2015), 9 Siqueira-Mello et al. (2015), 10 Ramírez et al. (2012), 11 Delgado Mena et al. (2015), 12 Delgado Mena et al. (2014), 13 Placco et al. (2016), 14 Bonifacio & Molaro (1997), 15 Boesgaard et al. (2011), 16 Smiljanic et al. (2009), 17 Rich & Boesgaard (2009), 18 Tan et al. (2009), 19 Roederer et al. (2014), 20 Meléndez et al. (2010), 21 Charbonnel & Balachandran (2000), 22 Hosford et al. (2009) Aguilera-Gómez et al. (2018). The oxygen abundances are from Boesgaard et al. (2011) or Smiljanic et al. (2009), in this latter case [O/H] is inferred by their $[\alpha\text{-element/Fe}]$.

Gaia source_id	Name	T_{eff}	$\log(g)$	[Fe/H]	[O/H]	A(Li)	[Fe/H] $_{Be}$	ϵ_{Fe}	A(Be)	ϵ_{Be}	ref
6086864760409366656	TYC 8248-1737-1	5901	4.05	-0.89		2.31					1
4725550450463451904	L 126-11	5857	3.79	-1.02		1.87					1
5459976109889190144	TYC 7174-224-1	5929	4.02	-1.12		1.85					1
5750434405835685888		5834	3.84	-1.16		2.35					1
6679323239394561792		5888	4.06	-1.16		2.23					1
5946574193490564480		5982	3.83	-1.17		2.28					1
5781595596159463040	TYC 9429-2667-1	5935	3.92	-1.21		1.95					1
6383892436469819008		5740	4.05	-1.23		2.19					1
6729270234418615552	CD-38 13129	5956	3.96	-1.24		2.01					1
5242632244811706496	TYC 9213-2091-1	5986	3.9	-1.3		2.3					1
3155410389590889856	G 89-14	5834	3.8	-1.32		2.32					1
32655224762711936	G4-36	5810	3.7	-2.17		1.98					19
3846427888295815552	HE0938+0114	6030	3.7	-3.09	-2.5	2.04	-2.67	0.11	-1.0	0.12	19,17
866863321051682176	BD+24 1676	6140	3.8	-2.7	-1.94	2.1	-2.55	0.09	-1.28	0.12	19,15
1289512635833404032	G166-47	5960	3.7	-2.46		2.12					19,15
4761346872572913408	HIP 24316	5725	4.4	-1.5	-1.33	2.12	-1.5	0.15	0.04	0.13	
5181063205724188032	G75-56	6190	3.9	-2.35	-1.74	2.23	-2.38	0.08	-0.84	0.12	19,15
1776289248313154688	BD+17 4708	6025	4.0	-1.61	-1.09	2.25	-1.5	0.15	-0.34	0.13	2,15
2658240166703766016	BD+02 4651	6100	3.8	-1.75	-1.18	2.36	-1.9	0.09	-0.58	0.12	2,15
4272653983123701120	G21-22	5916	4.6	-1.01	-1.02	2.48	-1.02	0.25	0.33	0.16	3,15
2910503176753011840	LTT2415.00	6295	4.1	-2.11		2.31					4
125750427611380480	G37-37	5990	3.8	-2.34		2.28					4
29331710349509376	G05-19	5942	4.2	-1.1	-0.62	2.26	-1.1	0.15	-0.01	0.13	5,15
2905773322545989760	HIP 25659	5855	4.5	-2.0		2.25					6
5586241315104190848	HD59392	5936	4.0	-1.61		2.24					7
5551565291043498496	CD-48 2445	6222	4.3	-1.93		2.22					7
949652698331943552	G107-50	6030	3.9	-2.06		2.2					19
5617037433203876224	W 0725-2351	6050	4.2	-2.55		2.17					8
870628736060892800	G88-10	6033	4.2	-2.53	-1.86	2.13	-2.61	0.07	-1.08	0.12	6,15
1097488908634778496	G234-28	5870	3.8	-1.8		2.1					19
6268770373590148224	HD 140283	5750	3.7	-2.5	-1.72	2.14	-2.41	0.08	-0.94	0.14	9,15
731253779217024640	HIP 52771	5937	4.5	-1.85	-1.4	2.22	-1.8	0.15	-0.55	0.13	10,16
791249665893533568	BD+51 1696	5725	4.6	-1.19	-0.53	1.9	-1.21		-0.33		10,15
2279933915356255232	BD+75 839	5770	4.0	-0.99		2.0					10
2427069874188580480	HIP 3026	6223	4.2	-1.11	-0.81	2.57	-1.2	0.15	-0.11	0.13	10
5486881507314450816	HIP 34285	5928	4.3	-0.88	-0.25	2.23	-0.9	0.15	0.15	0.13	11,16
6859076107589173120	HIP 100568	5801	4.6	-1.0	-0.65	1.93	-1.0	0.15	0.08	0.13	12,16
4468185319917050240	G 20-24	6190	3.9	-1.91	-1.41	2.19	-1.92	0.08	-0.72	0.17	18,16
4376174445988280576	BD +2 3375	5800	4.1	-2.39	-1.48		-2.39	0.17	-0.74	0.15	17,17
588856788129452160	BD 9 2190	6008	3.9	-3.0	-2.38	2.13	-3.0	0.09	-1.22	0.11	7,17
61382470003648896	G 5 -40	5863	4.2	-0.83	-0.60	1.9	-0.83	0.15	0.85	0.13	16,16
4715919175280799616	HIP 7459	5909	4.46	-1.15	-0.98	2.12	-1.15	0.15	0.12	0.13	16,16
3643857920443831168	G64-37	6300	4.2	-3.22	-2.32	2.25	-3.28	0.05	-1.4	0.11	13,15
5709390701922940416	HIP 42592	6040	4.1	-2.17	-1.56	2.24	-2.0	0.15	-0.58	0.13	14,16
5184824046591678848	LP 651-4	6030	4.3	-2.89	-2.04		-2.89	0.08	-1.12	0.12	17,17
761871677268717952	BD 36 2165	6315	4.3	-1.38		2.42					20
2722849325377392384	BD 7 4841	5922	3.9	-1.25		2.22					21
16730924842529024	BD 11 468	5739	4.6	-1.55		1.85					20
1458016709798099952	BD 34 2476	6416	4.0	-2.07		2.3					20
5806792348219626624	CD -71 1234	6194	4.5	-2.55		2.21					22
3699174968912810624	HE1208-0040	6304	4.3	-2.08		2.38					20
4228176122142169600	G 24-25	5752	3.7	-1.56	-0.98		-1.56	0.09	-0.73	0.12	15,15
5133305707717726464	BD -17 484	6110	3.6	-1.56	-0.95		-1.56	0.09	-0.37	0.12	15,15

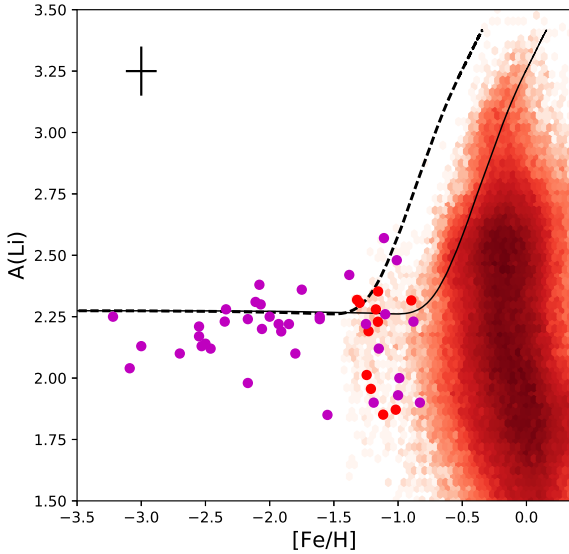


Figure 1. Li abundances $A(\text{Li})$ as a function of $[\text{Fe}/\text{H}]$ of all dwarf Gaia-Enceladus candidates with ($\log g > 3.65$, $T_{\text{eff}} > 5700$ K) found in the GALAH survey, red dots, and in literature, magenta, listed in Table 2. The GALAH stars have recommended stellar parameters (flag cannon=0) ${}^7\text{Li}$ abundance. The cross in the top left corner shows a typical $\pm\sigma$ abundance error. The best model of the Li evolution for the thin disc presented in Cescutti & Molaro (2019) is shown in black solid line. With a black dashed line is the same model but shifted by -0.5 dex in metallicity as a proxy for the time delay expected for a dwarf galaxy as Gaia-Enceladus.

that is efficiently burned at a temperature of several millions degrees, both a dilution with the ${}^7\text{Li}$ free hot interior material and some ${}^7\text{Li}$ burning at the bottom of the surface convective zone make the ${}^7\text{Li}$ abundance in a giant star decrease by $\sim 1.3 - 1.5$ dex below its main sequence value. Some extra mixing after the RGB bump reduces the surface ${}^7\text{Li}$ abundance to an even lower value (Charbonnel & Zahn 2007). The $A(\text{Li})$ vs. $\log g$ evolution of the Gaia-Enceladus stars is shown in Figure 2 where the $\log g$ is considered an index of the evolutionary phase. The giant stars show the characteristic depletion flattening at $A(\text{Li}) \approx 1.3$ and with a minor fraction showing the sign of extra-mixing with almost no ${}^7\text{Li}$ after $\log g \approx 1.8$. $A(\text{Li})$ measured in red giants is in good agreement with the results for the Galactic halo field, e.g. Mucciarelli et al. (2012) found an average of $A(\text{Li}) = 0.97$ for the Milky Way halo stars.

In the Galaxy there is a small fraction of giants with relatively large $A(\text{Li})$ abundances $\gtrsim 2.0$, i.e. the Li-rich giants. This lithium could be produced if there were extra mixing by a Cameron-Fowler mechanism, which requires some ${}^7\text{Be}$ produced in the stellar interior and transported to the stellar surface by convection where it decays into ${}^7\text{Li}$ (Cameron & Fowler 1971; Sackmann & Boothroyd 1999). Another possibility is that Li has been preserved instead of undergoing post main-sequence dilution. The precise mechanism is controversial and it is not clear if there is net production of ${}^7\text{Li}$ or merely a preservation of the initial one (Casey et al. 2016).

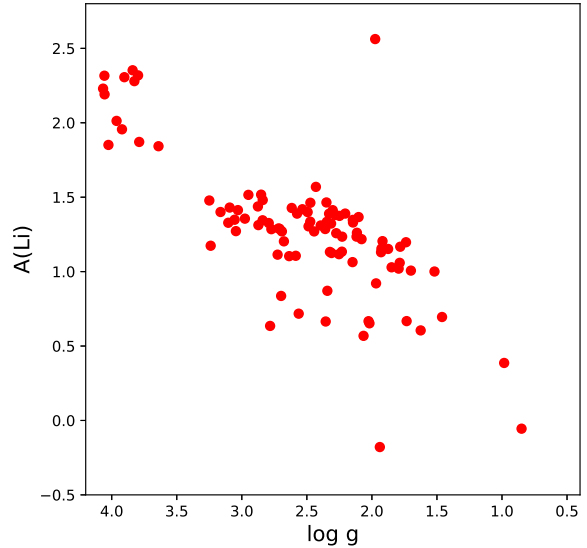


Figure 2. ${}^7\text{Li}$ abundances of all the Gaia-Enceladus star candidates from the GALAH survey.

Several recent giant stars have been detected Li et al. (e.g. 2018); Yan et al. (e.g. 2018); Smiljanic et al. (e.g. 2018); Gao et al. (e.g. 2019), including one with very high abundance. However, this star is still in the main sequence or has just left it, and its high abundance is quite anomalous. It is therefore interesting to see whether Li-rich giants are present in other galaxies (e.g. Kirby et al. 2012). In our sample of 121 Gaia-Enceladus candidates drawn from GALAH and shown in Figure 2, there is one star 15344465-3331196 ($T_{\text{eff}} = 4837$ K, $\log g = 1.97$, $[\text{Fe}/\text{H}] = -0.37$) with $A(\text{Li}) \approx 2.6$, out of 101 stars with $\log g \leq 3.65$. Therefore, in Gaia-Enceladus the fraction of ${}^7\text{Li}$ rich giants is of about 1%, very close to the 1-2% found in the Galaxy. Casey et al. (2019) argue that Li rich giants are likely binary systems in the red clump. However, Adamów et al. (2018) monitored a sample of 15 Li-rich giants within a Planet-Search program and found a normal binary fraction. The Casey et al. (2019) suggestion still requires a full observational investigation, but it would be interesting to investigate if the Li-rich giant found in Gaia-Enceladus is also a binary system.

4 BERYLLIUM ABUNDANCES IN GAIA-ENCELADUS

${}^9\text{Be}$ is burnt in the interior of the stars and is made through Galactic Cosmic Ray (GCR) spallation reactions in the interstellar medium (Reeves et al. 1970; Meneguzzi et al. 1971). Energetic cosmic rays with energies > 100 MeV hit CNO atoms at rest in the ambient interstellar gas and break them into smaller pieces, producing Li, Be and B. A reverse mechanism is working also during supernovae explosions which accelerate nuclei of C, N, and O which later collide with protons and α particles in the surrounding medium and break up into smaller units. The only suitable transi-

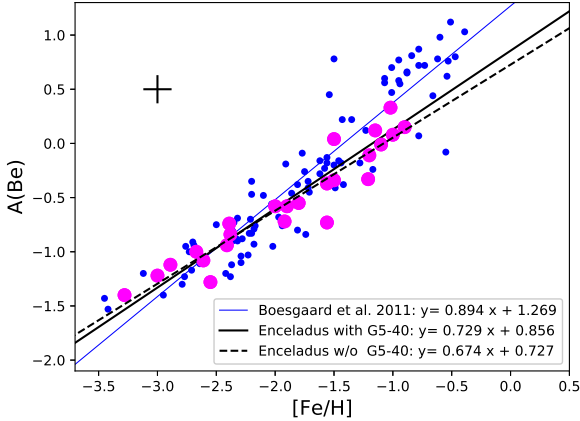


Figure 3. $A(\text{Be})$ abundances versus iron abundances. $A(\text{Be})$ abundances from Boesgaard et al. (2011) are in blue dots. The Gaia-Enceladus star candidates are highlighted in magenta, with a squared symbol for G5-40. The cross on the top left corner shows the mean errors in the abundances reported in Table 2. The solid and dashed black lines are the best fit through the Gaia-Enceladus stars with and without G5-40, respectively. The solid blue line is the best fit through the Boesgaard et al. (2011) data points without Gaia-Enceladus candidates.

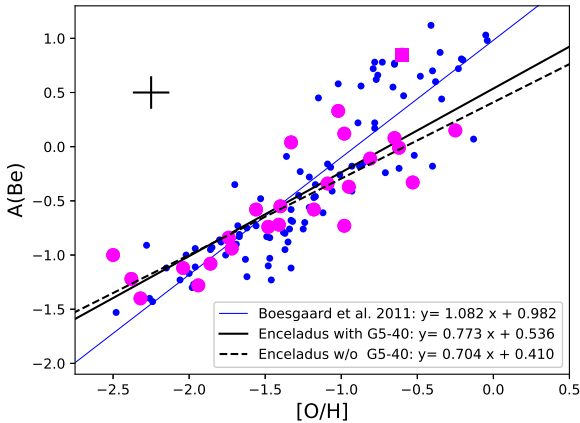


Figure 4. $A(\text{Be})$ abundances versus oxygen abundances. Symbols and lines are the same as in Figure 3.

tions of beryllium are the $^9\text{BeII}$ resonance lines which fall at 313.0 nm close to the atmospheric cut off. For this reason ^9Be is a very challenging element to be measured in Galactic halo stars (Molaro & Beckman 1984; Molaro et al. 1997; Smiljanic et al. 2009; Boesgaard et al. 2011). In extragalactic stars it will probably remain out of reach also for the next generation of giant 40 m class telescopes. However, few stars belonging to Gaia-Enceladus have measured ^9Be and arguably these could be arguably considered as the first extragalactic ^9Be measurements.

These 25 stars are listed in Table 2 and are shown in Figure 3 together with the Galactic measurements. The ^9Be

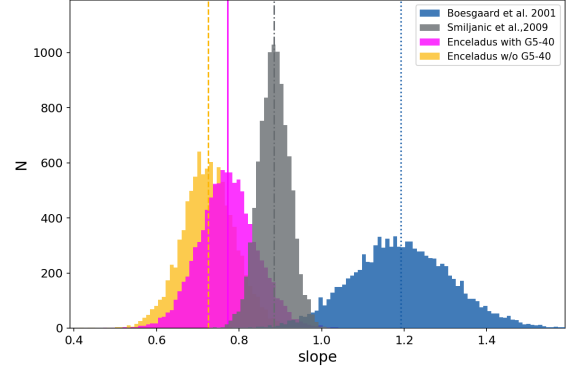


Figure 5. Distribution of the slopes from a linear fitting with a MCMC of 10000 chains. The median slope value of each data set is marked with vertical line: blue dotted line for Boesgaard et al. (2011), grey dash-dot line for Smiljanic et al. (2009), magenta solid line for Enceladus with G5-40, and yellow dashed line for Enceladus without G5-40.

abundance in these stars shares the same location of the Galactic stars but lay preferentially at lower ^9Be abundances for a given metallicity. Figure 3 shows the relationship between $[\text{Fe}/\text{H}]$ and $A(\text{Be})$ for the Gaia-Enceladus stars together with the data points from Boesgaard et al. (2011). We found that the linear fit between these two logarithmic quantities for the Gaia-Enceladus stars is:

$$A(\text{Be}) = 0.729(\pm 0.059)[\text{Fe}/\text{H}] + 0.856(\pm 0.117) \quad (1)$$

When G5-40 is not considered slope and intercept become 0.674 ± 0.048 and 0.727 ± 0.098 , respectively with a dispersion of 0.16 dex. The regression found for the Gaia-Enceladus candidate stars is significantly different than that found with Boesgaard et al. (2011) data points. After taking out the 17 data points in common with Gaia-Enceladus sample, the remaining 98 measurements provide the relation:

$$A(\text{Be}) = 0.894(\pm 0.041)[\text{Fe}/\text{H}] + 1.269(\pm 0.078) \quad (2)$$

The two slopes and intercepts differ by 2.3σ , 3.5 without G5-40, and 2.9 (3.5) σ , respectively. However, it seems that this difference is mainly produced by the Galactic $A(\text{Be})$ measurements for $[\text{Fe}/\text{H}] > -1$. Smiljanic et al. (2009) found an even steeper slope but with a smaller number of very metal-poor stars. For stars with $[\text{Fe}/\text{H}] > -2.2$, the slope is of 1.04 ± 0.06 in Boesgaard et al. (2011) and 1.16 ± 0.07 found by Smiljanic et al. (2009).

To asses with confidence that we deal with two different populations, we have performed a MCMC (following the method described in Kelly 2007) of the $A(\text{Be})$ vs $[\text{Fe}/\text{H}]$ by taking into account the errors reported in Table 2. The MCMC result with 10000 chains for the Gaia-Enceladus values is $A(\text{Be}) = 0.770(\pm 0.070)[\text{Fe}/\text{H}] + (0.957 \pm 0.140)$. The slope is slightly flatter if star G5-40 is not considered: $A(\text{Be}) = 0.725(\pm 0.065)[\text{Fe}/\text{H}] + (0.845 \pm 0.133)$. While the MCMC fitting for the Boesgaard et al. (2011) and Smiljanic et al. (2009) samples, once cleaned from the Enceladus candidate stars, are $A(\text{Be}) = 0.884(\pm 0.038)[\text{Fe}/\text{H}] + 1.245(\pm 0.075)$ and $A(\text{Be}) = 1.186(\pm 0.121)[\text{Fe}/\text{H}] + 1.587(\pm 0.126)$, respectively. In

Figure 5 are shown the distribution of the slope values of the Gaia-Enceladus candidates, the [Boesgaard et al. \(2011\)](#) and [Smiljanic et al. \(2009\)](#) stars. The slope of the Gaia-Enceladus candidates stars, no matter if star G5-40 has been taken into account, is flatter than that of [Boesgaard et al. \(2011\)](#) and [Smiljanic et al. \(2009\)](#). We apply a two-side K-S statistic to check the significance of the slope difference. The result shows a zero probability that the MCMC slope distribution between the Gaia-Enceladus stars and the [Boesgaard et al. \(2011\)](#); [Smiljanic et al. \(2009\)](#) are similar. However, the main cause of the difference with [Smiljanic et al. \(2009\)](#) is probably due to the fact that they have much fewer stars at low metallicity.

We note that there is considerable overlap of the $A(\text{Be})$ abundances at the low metallicity end between Gaia-Enceladus and the MW. For instance, the average of 6 stars in the Gaia-Enceladus sample with metallicity $[\text{Fe}/\text{H}] < -2.2$ provides $\langle A(\text{Be}) \rangle = -1.18$ at $\langle [\text{Fe}/\text{H}] \rangle = -2.83$. In the [Boesgaard et al. \(2011\)](#) there are 15 stars in this metallicity range with $\langle A(\text{Be}) \rangle = -1.17$ and $\langle [\text{Fe}/\text{H}] \rangle = -2.86$. Since they share the same mean values at low metallicities, to evaluate a different growth we considered the lines passing through it $A(\text{Be}) = -1.17 + a([\text{Fe}/\text{H}] + 2.85)$, and fitted the remaining points of the two data samples. The results are $a = 0.695(\pm 0.034)$, or $a = 0.658(\pm 0.028)$ without G5-40, for Gaia-Enceladus and $a = 0.825(\pm 0.023)$ for the [Boesgaard et al. \(2011\)](#) cleaned sample. The two slopes differ by 3.17, or 4.6 without G5-40 σ , and confirm the different growth in the two populations. To further test that this result is not casual we took 10000 samples of 25 stars randomly drawn from the sample of 115 stars in [Boesgaard et al. \(2011\)](#) sample. The distribution of the slopes is provided in Figure 7. They show a mean of $a = 0.802 \pm 0.056$ differing by 2.3σ from that of Gaia-Enceladus without G5-40.

As mentioned before, ^9Be production is directly related to oxygen rather than to iron. Therefore, we show in Fig. 4 the available determinations for beryllium and oxygen reported in Table 2. We have also calculated the correlations for Gaia-Enceladus:

$$A(\text{Be}) = 0.536(\pm 0.105)[\text{O}/\text{H}] + 0.773(\pm 0.153) \quad (3)$$

with a dispersion of 0.30, or $A(\text{Be}) = 0.385(\pm 0.139) + 0.700(\pm 0.0937)[\text{O}/\text{H}]$ without G5-40, with a dispersion of 0.26 dex. The analysis of the remaining 98 data points in [Boesgaard et al. \(2011\)](#) provides:

$$A(\text{Be}) = 1.082(\pm 0.0642)[\text{O}/\text{H}] + 0.982(\pm 0.0854) \quad (4)$$

with a dispersion of 0.36. Although the data points are slightly more scattered, probably due to the difficulty of the oxygen determination, the regression analysis shows a flatter and less scattered slope for the Gaia-Enceladus candidates stars in comparison with that of the Milky Way.

[Smiljanic et al. \(2009\)](#) found statistical evidence for an intrinsic scatter in the halo stars in the $A(\text{Be})$ - $[\text{Fe}/\text{H}]$ relation, above what is expected from observational errors. The observed scatter in the Galaxy is of the order of 0.5 dex. while the dispersion of the ^9Be abundances in Gaia-Enceladus stars is of 0.19 dex, which is comparable to the measurement errors. For comparison the dispersion of the data point along the fit of the 98 data points in [Boesgaard et al. \(2011\)](#) is 0.298 dex, i.e. almost a factor two larger

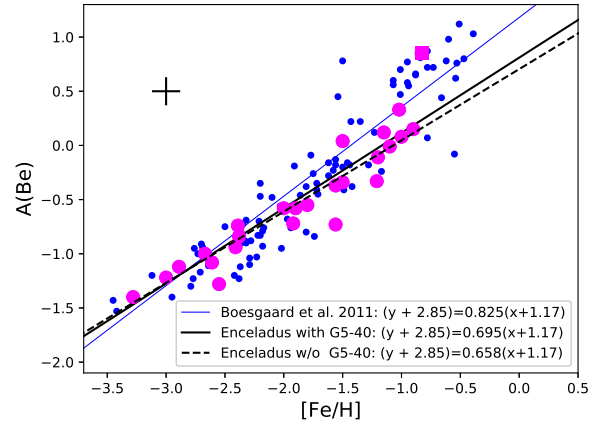


Figure 6. Best fit for Gaia-Enceladus and Milky Ways data points for the family of lines passing through the common origin: $[\text{Fe}/\text{H}] = -2.85$, $A(\text{Be}) = -1.17$. Symbols as in Figure 3.

than the data of the Gaia-Enceladus candidates. The uncertainties in the $A(\text{Be})$ abundance determination comes from the atmospheric parameters, mainly the $\log g$, and from the location of the pseudo-continuum and unidentified blends. The total uncertainty is of ≈ 0.15 dex, which is of the same order of the observed dispersion in Gaia-Enceladus stars.

Overall the $A(\text{Be})$ versus $[\text{Fe}/\text{H}]$ behaviour of Gaia-Enceladus seems to belong to a very homogeneous stellar population with a very smooth beryllium enrichment. On the other hand the scatter observed in the Galaxy could be originated by the presence of multiple stellar populations with different time scales in the ^9Be evolution as has been also suggested by [Smiljanic et al. \(2009\)](#).

[Rich & Boesgaard \(2009\)](#) found that the dependence of $A(\text{Be})$ on $[\text{Fe}/\text{H}]$ shows distinct differences in the accretive group of Galactic stars. The latter show a flatter slope of $A(^9\text{Be})$ with $[\text{Fe}/\text{H}]$ than the Galactic stars. They ascribe this different behaviour to the differing importance of the two mechanisms for ^9Be formation, i.e. in the vicinity of SN II stars or preferentially by GCR spallation reaction. [Rich & Boesgaard \(2009\)](#) found that the accretive and retrograde groups show $A(\text{Be}) \leq 0.35$ and the star G21-22 with $A(\text{Be}) = 0.31$ is the highest value. We note that G 5-40, the most metal rich star in our sample of Gaia-Enceladus candidates, shows $A(\text{Be}) = 0.85$. However, this star is a bit out to the general trend in the Be-metallicity plot. Thus, it would be of interest if a similar cut found for the accretive stars applied also to Gaia-Enceladus. This would be possible by searching for $^9\text{Be II}$ in other metal rich stars of the Gaia-Enceladus galaxy. As we have seen omitting G 5-40 from the Gaia-Enceladus bona fide candidates makes the difference between Gaia-Enceladus and the Galaxy more significant.

5 DISCUSSION

Among the light Big Bang elements D and ^4He are observed in extragalactic objects. Most of the ^4He measures come from the local universe at redshifts typically of 0.01 to 0.1 at most while Deuterium is observed up to a redshift of 3

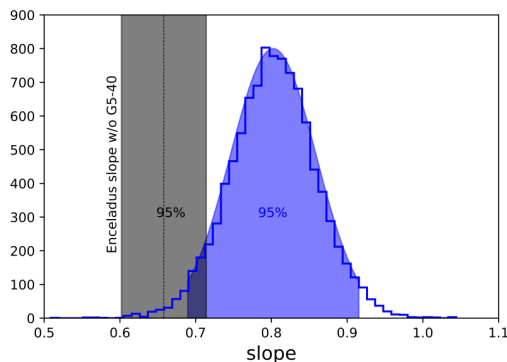


Figure 7. Distribution of slopes for 10000 samples of 25 stars randomly drawn from the 115 stars of Boesgaard et al. (2011). The slope refers to the family of lines passing through the common origin: $[\text{Fe}/\text{H}] = -2.85$, $A(\text{Be}) = -1.17$. The slope of the Gaia-Enceladus star candidates without G5-40 is also shown.

or even 4. ^3He can be measured only in the Galaxy (Banja et al. 2010) and the same applies to ^7Li since main sequence solar type stars in external galaxies are out of reach even for the 10m class telescopes. Upper limits for the interstellar Li towards the SN1987A in the LMC were obtained when the supernova was as bright as $V \approx 4$ mag (Molaro & Vladilo 1989). A detection of interstellar ^7Li has been reported by Howk et al. (2012) in the SMC in the line of sight towards the star SK143.

Molaro et al. (1997) suggested that Li could have been detected in Galactic stars, which might possibly have been born in other galaxies. Preston et al. (1994) in their HK objective prism survey of metal poor stars in the Milky Way identified a population of stars which they called the blue metal poor main sequence stars (BMP). This population is composed by hot and metal poor objects that should have already evolved from the main sequence if coeval with the halo stars. The space density for the BMP stars is about one order of magnitude larger than that of blue stragglers in globular cluster, thus suggesting that field BS are a minor component of this population. Moreover, the kinematical properties of the BMP are intermediate among those of halo and thick-disk populations. In Preston et al. (1994), the authors suggested that the BMP population has been accreted from a low luminosity satellite of the Milky Way in the recent past. One of these stars is CS 22873-139 which has a remarkably low metallicity $[\text{Fe}/\text{H}] = -3.1$. This object is a spectroscopic binary for which Preston et al. (1994) derived an age of < 8 Gyr, which again is too short for an halo star. Li abundance in star CS 22873-139 has the canonical halo value of $A(\text{Li}) = 2.28$.

Recently several efforts have been made to measure *extragalactic* ^7Li abundance. Omega Centauri is a globular cluster-like stellar system characterized by a wide range of metallicities and probably of ages, and probably was stripped from the core of a dwarf galaxy. Monaco et al. (2010) found that Ω Cen dwarfs display a constant Li abundance observed among the stars spanning a wide range of ages and metallicities that overlap with the Spite plateau. Mucciarelli et al. (2014) by means of stellar modeling have been able to derive the initial lithium abundance in the globular cluster M54 in the nucleus of the Sagittarius dwarf

galaxy. The Sagittarius galaxy is at 25 Kpc and the main sequence stars are of 22 mag and too faint to be studied at high resolution. The only possibility are Red Giant Branch stars where the ^7Li abundance has been modified by a post MS dilution. By considering dilution Mucciarelli et al. (2014) have established an initial Li abundance of this stellar system ($A(\text{Li}) = 2.29 \pm 0.11$ or 2.35 ± 0.11 dex, when accounting also for atomic diffusion).

The analysis of the Gaia-Enceladus stars confirms the discrepancy between the primordial nucleosynthesis prediction and the metal poor stars of this dwarf galaxy suggesting that the Li cosmological problem is ubiquitous and present also in other galaxies, regardless of their type. Thus, a solution able to explain the discrepancy must work both in the Milky Way and for other galaxies, with likely experienced different origins and star formation histories. As noted by Mucciarelli et al. (2014), it is unlikely that the scenario proposed by Piau et al. (2006), requiring one third of the gas in the Galactic halo re-processed by Population III massive stars, could be valid also in a smaller galactic system such as Gaia-Enceladus.

For a chemical evolution model which assume that lithium is mainly produced by novae it is expected that a dwarf galaxy like Gaia-Enceladus the Li abundance will rise from the Spite plateau at a metallicity lower than in the Galactic thin disk. Future observations targeting hot dwarf stars of Gaia-Enceladus with metallicity in the range ≈ -1.5 , -1.0 will allow to establish the presence of a slightly different Li evolutionary behaviour.

The formation of ^9Be occurs during supernovae explosions when CNO atoms accelerate out into the ambient gas and strike protons and neutrons splitting into smaller atoms. An interesting feature is the fact that the ^9Be abundances of Gaia-Enceladus stars starting from the same origin at the lowest metallicities, then show a more gentle rise and the tendency to populate the lower region of the Galactic halo stars. A possible explanation is that SNe Ia contributed to the abundance of iron of the Gaia-Enceladus stars. The relative contribution of SNe Ia to Fe is higher in a low star formation galaxy as Gaia-Enceladus compared to the Milky Way. This would produce an enhancement in iron without a corresponding ^9Be production and, therefore, a smaller ^9Be abundance in Gaia-Enceladus for a given metallicity is expected. However, if this is the case the Be-O relations should not differ. Alternatively, there could be a steeper increase of $A(\text{Be})$ in the Galaxy for $[\text{Fe}/\text{H}] \geq -1.5$ possibly due to an increase in importance of the inverse spallation process at high metallicity. This phase is marginally seen in Enceladus and the two relations could appear different when fitting onto the whole metallicity range.

^9Be is only produced by spallation of cosmic rays and its abundance allows to constrain the degree to which ^7Li , ^6Li , ^{11}B and ^{10}B may have been produced by the same processes. Thus, the amount of ^7Li and ^6Li produced by spallation of high energy cosmic rays in the Gaia-Enceladus can be inferred from the observed Be by taking the ratio of the cross sections of spallation processes ($^7\text{Li}/^9\text{Be} = 7.6$ and $^6\text{Li}/^9\text{Be} = 5.5$ (Steigman & Walker 1992)). Observationally it is not possible to resolve ^6Li from ^7Li and they both are considered contributing to the Li 670.7 nm line. However, ^6Li is rather fragile and is not expected to survive in halo stars where it is not detected. Therefore, we consider only the $^7\text{Li}/^9\text{Be}$ rel-

ative cross section, providing 7.6 (Molaro et al. 1997). The predicted fraction of Li produced by spallation processes in Gaia-Enceladus should follow a relation with similar slope but shifted by 0.88 dex. The low ^9Be abundance in Gaia-Enceladus implies a relatively small contribution by spallation processes to the Li observed in Gaia-Enceladus stars. These abundances are virtually extragalactic measurements of ^9Be and therefore hold a more general significance.

Besides standard galactic cosmic rays, it has been suggested that additional production of light elements might come from cosmic rays accelerated in galaxy-galaxy interactions (Prodanović et al. 2013). In support of this possibility are produced the high lithium values in the ISM of M82 (Ritchey et al. 2015) and the high $^6\text{Li}/^7\text{Li}$ ratio in the SMC of (Howk et al. 2012). Within a simplified framework Prodanović et al. (2013) showed that large-scale tidal shocks from a few galactic fly-bys can possibly produce light elements in amounts comparable to those expected from the interactions of galactic cosmic-rays produced in supernovae over the entire history of a system. These effects are particularly evident for dwarf galaxies. In the case of the SMC, they found that only two such fly-bys could account for as much lithium as the standard galactic cosmic ray production channel. The same processes should lead to an additional amount of ^9Be and in particular in dwarf galaxies such as Gaia-Enceladus which suffered the tidal collision that resulted into the merging with the Galaxy. The observations of Gaia-Enceladus do not reveal any excess of ^9Be compared to the Galaxy and restrict the possibility of an additional ^9Be nucleosynthetic channel. However, in case of a head-on collision with a direct merger no extra production of the light elements is expected.

6 ACKNOWLEDGEMENTS

We thank Alexandro Saro for his advice regarding statistical tests and acknowledge useful discussions with Tijana Prodanovic on the effects of tidal production of light elements. We warmly thank an anonymous referee for several suggestions which improved the paper significantly. The use of TOPCAT tool (Taylor 2005), the Simbad database and the Vizier catalog access tool of CDS (Ochsenbeim et al. 2000) are also acknowledged. This work has been partially supported by the EU COST Action CA16117 (ChETEC). XF acknowledges the support of the National Natural Science Foundation of China under grant number 11973001 and National Key R&D Program of China No. 2019YFA0405504. The GALAH survey is based on observations made at the Australian Astronomical Observatory, under programmes A/2013B/13, A/2014A/25, A/2015A/19, A/2017A/18. We acknowledge the traditional owners of the land on which the AAT stands, the Gamilaraay people, and pay our respects to elders past and present.

REFERENCES

Abomalima A., Frebel A., 2018, *ApJS*, **238**, 36
Adamów M., Niedzielski A., Kowalik K., Villaver E., Wolszczan A., Maciejewski G., Gromadzki M., 2018, *A&A*, **613**, A47
Aguilera-Gómez C., Ramírez I., Chanamé J., 2018, *A&A*, **614**, A55

Asplund M., Lambert D. L., Nissen P. E., Primas F., Smith V. V., 2006, *ApJ*, **644**, 229
Bania T. M., Rood R. T., Balser D. S., 2010, in Charbonnel C., Tosi M., Primas F., Chiappini C., eds, IAU Symposium Vol. 268, Light Elements in the Universe. pp 81–90, doi:10.1017/S174392131000390X
Belokurov V., Erkal D., Evans N. W., Koposov S. E., Deason A. J., 2018, *MNRAS*, **478**, 611
Boesgaard A. M., Novicki M. C., 2006, *ApJ*, **641**, 1122
Boesgaard A. M., Stephens A., Deliyannis C. P., 2005, *ApJ*, **633**, 398
Boesgaard A. M., Rich J. A., Levesque E. M., Bowler B. P., 2011, *ApJ*, **743**, 140
Bonifacio P., Molaro P., 1997, *MNRAS*, **285**, 847
Brook C. B., Kawata D., Gibson B. K., Flynn C., 2003, *ApJ*, **585**, L125
Buder S., et al., 2018, *MNRAS*, **478**, 4513
Burbidge E. M., Burbidge G. R., Fowler W. A., Hoyle F., 1957, *Reviews of Modern Physics*, **29**, 547
Cameron A. G. W., Fowler W. A., 1971, *ApJ*, **164**, 111
Casey A. R., et al., 2016, *MNRAS*, **461**, 3336
Casey A. R., et al., 2019, *ApJ*, **880**, 125
Cescutti G., Molaro P., 2019, *MNRAS*, **482**, 4372
Cescutti G., Molaro P., Fu X., 2020, arXiv e-prints, p. arXiv:2004.06606
Charbonnel C., Balachandran S. C., 2000, *A&A*, **359**, 563
Charbonnel C., Primas F., 2005, *A&A*, **442**, 961
Charbonnel C., Zahn J.-P., 2007, *A&A*, **467**, L15
Delgado Mena E., et al., 2014, *A&A*, **562**, A92
Delgado Mena E., et al., 2015, *A&A*, **576**, A69
Duncan D. K., Lambert D. L., Lemke M., 1992, *ApJ*, **401**, 584
Fields B. D., 2011, *Annual Review of Nuclear and Particle Science*, **61**, 47
Fields B. D., Molaro P., Sarkar S., 2014, preprint (arXiv:1412.1408)
Fu X., Bressan A., Molaro P., Marigo P., 2015, *MNRAS*, **452**, 3256
Fulbright J. P., 2000, *AJ*, **120**, 1841
Gaia Collaboration et al., 2016, *A&A*, **595**, A1
Gao Q., Shi J.-R., Yan H.-L., Yan T.-S., Xiang M.-S., Zhou Y.-T., Li C.-Q., Zhao G., 2019, *ApJS*, **245**, 33
Gilmore G., et al., 2012, *The Messenger*, **147**, 25
Gratton R. G., Carretta E., Desidera S., Lucatello S., Mazzei P., Barbieri M., 2003, *A&A*, **406**, 131
Haywood M., Di Matteo P., Lehnert M. D., Snaith O., Khoperskov S., Gómez A., 2018, *ApJ*, **863**, 113
Helmi A., Babusiaux C., Koppelman H. H., Massari D., Veljanoski J., Brown A. G. A., 2018, *Nature*, **563**, 85
Hosford A., Ryan S. G., García Pérez A. E., Norris J. E., Olive K. A., 2009, *A&A*, **493**, 601
Howk J. C., Lehner N., Fields B. D., Mathews G. J., 2012, *Nature*, **489**, 121
Ibata R., Irwin M., Lewis G., Ferguson A. M. N., Tanvir N., 2001, *Nature*, **412**, 49
Izzo L., et al., 2018a, *MNRAS*, **478**, 1601
Izzo L., et al., 2018b, *The Astronomer's Telegram*, **11468**
Kelly B. C., 2007, *ApJ*, **665**, 1489
Kirby E. N., Guhathakurta P., Bolte M., Sneden C., Geha M. C., 2009, *ApJ*, **705**, 328
Kirby E. N., Fu X., Guhathakurta P., Deng L., 2012, *ApJ*, **752**, L16
Korn A. J., Grundahl F., Richard O., Barklem P. S., Mashonkina L., Collet R., Piskunov N., Gustafsson B., 2006, *Nature*, **442**, 657
Li H., Aoki W., Matsuno T., Bharat Kumar Y., Shi J., Suda T., Zhao G., 2018, *ApJ*, **852**, L31
Matteucci F., Brocato E., 1990, *ApJ*, **365**, 539
McMillan P. J., 2017, *MNRAS*, **465**, 76

- Meléndez J., Casagrande L., Ramírez I., Asplund M., Schuster W. J., 2010, *A&A*, **515**, L3
- Meneguzzi M., Audouze J., Reeves H., 1971, *A&A*, **15**, 337
- Molaro P., 2006, Abundances in Damped Ly α Galaxies. p. 256, doi:10.1007/978-3-540-34136-9_84
- Molaro P., Beckman J., 1984, *A&A*, **139**, 394
- Molaro P., Vladilo G., 1989, *Ap&SS*, **156**, 107
- Molaro P., Bonifacio P., Castelli F., Pasquini L., 1997, *A&A*, **319**, 593
- Molaro P., Izzo L., Mason E., Bonifacio P., Della Valle M., 2016, *MNRAS*, **463**, L117
- Monaco L., Bonifacio P., Sbordone L., Villanova S., Pancino E., 2010, *A&A*, **519**, L3
- Mucciarelli A., Salaris M., Bonifacio P., 2012, *MNRAS*, **419**, 2195
- Mucciarelli A., Salaris M., Bonifacio P., Monaco L., Villanova S., 2014, *MNRAS*, **444**, 1812
- Nidever D. L., et al., 2012, *ApJ*, **755**, L25
- Nissen P. E., Schuster W. J., 2010, *A&A*, **511**, L10
- Ochsenbein F., Bauer P., Marcout J., 2000, *A&AS*, **143**, 23
- Piau L., Beers T. C., Balsara D. S., Sivarani T., Truran J. W., Ferguson J. W., 2006, *ApJ*, **653**, 300
- Pinsonneault M. H., Narayanan V. K., Steigman G., Walker T. P., 1998, in Donahue R. A., Bookbinder J. A., eds, *Astronomical Society of the Pacific Conference Series Vol. 154, Cool Stars, Stellar Systems, and the Sun*. p. 959 ([arXiv:astro-ph/9710035](#))
- Placco V. M., Beers T. C., Reggiani H., Meléndez J., 2016, *ApJ*, **829**, L24
- Preston G. W., Beers T. C., Shectman S. A., 1994, *AJ*, **108**, 538
- Prodanović T., Bogdanović T., Urošević D., 2013, *Phys. Rev. D*, **87**, 103014
- Rafelski M., Wolfe A. M., Prochaska J. X., Neeleman M., Mendez A. J., 2012, *ApJ*, **755**, 89
- Ramírez I., Fish J. R., Lambert D. L., Allende Prieto C., 2012, *ApJ*, **756**, 46
- Rebolo R., Beckman J. E., Molaro P., 1988, *A&A*, **192**, 192
- Reeves H., Fowler W. A., Hoyle F., 1970, *Nature*, **226**, 727
- Rich J. A., Boesgaard A. M., 2009, *ApJ*, **701**, 1519
- Ritchey A. M., Welty D. E., Dahlstrom J. A., York D. G., 2015, *ApJ*, **799**, 197
- Roederer I. U., Preston G. W., Thompson I. B., Shectman S. A., Sneden C., Burley G. S., Kelson D. D., 2014, *AJ*, **147**, 136
- Sackmann I. J., Boothroyd A. I., 1999, *ApJ*, **510**, 217
- Sbordone L., et al., 2010, *A&A*, **522**, A26
- Siqueira-Mello C., Andrievsky S. M., Barbay B., Spite M., Spite F., Korotin S. A., 2015, *A&A*, **584**, A86
- Smiljanic R., Pasquini L., Bonifacio P., Galli D., Gratton R. G., Randich S., Wolff B., 2009, *A&A*, **499**, 103
- Smiljanic R., et al., 2018, *A&A*, **617**, A4
- Spite M., Spite F., Caffau E., Bonifacio P., 2015, *A&A*, **582**, A74
- Steigman G., Walker T. P., 1992, *ApJ*, **385**, L13
- Suda T., et al., 2008, *PASJ*, **60**, 1159
- Tajitsu A., Sadakane K., Naito H., Arai A., Aoki W., 2015, *Nature*, **518**, 381
- Tan K. F., Shi J. R., Zhao G., 2009, *MNRAS*, **392**, 205
- Taylor M. B., 2005, in Shopbell P., Britton M., Ebert R., eds, *Astronomical Society of the Pacific Conference Series Vol. 347, Astronomical Data Analysis Software and Systems XIV*. p. 29
- Tolstoy E., Hill V., Tosi M., 2009, *ARA&A*, **47**, 371
- Vincenzo F., Spitoni E., Calura F., Matteucci F., Silva Aguirre V., Miglio A., Cescutti G., 2019, *MNRAS*, **487**, L47
- Wagoner R. V., Fowler W. A., Hoyle F., 1967, *ApJ*, **148**, 3
- Yan H.-L., et al., 2018, *Nature Astronomy*, **2**, 790

This paper has been typeset from a \LaTeX file prepared by the author.

Table 2. Kinematical properties of the selected Gaia-Enceladus candidates. The energy (En) and the angular momentum in the z direction (Lz) are from [Helmi et al. \(2018\)](#). The apocenter distance (R_{APO}), the pericenter distance (R_{PER}), the max distance from the Galactic plane (Z_{max}) and the eccentricity (Ecc), are computed from the stellar orbit of the past 1 Gyr.

Gaia source_id	Name	Energy	Lz	r_{apo}	r_{peri}	ecc	Zmax
6086864760409366656	TYC 8248-1737-1	-156076.36	-183.31	16.07	0.72	0.91	0.93
4725550450463451904	L 126-11	-143328.41	73.65	20.79	0.24	0.98	1.13
5459976109889190144	TYC 7174-224-1	-177744.13	-332.32	10.57	1.09	0.81	0.27
5750434405835685888	–	-166586.73	-32.53	12.74	0.12	0.98	7.17
6679323239394561792	–	-160505.95	-552.18	14.46	1.37	0.83	1.60
5946574193490564480	–	-137327.40	-33.12	22.11	0.24	0.98	18.50
5781595596159463040	TYC 9429-2667-1	-179647.78	-1113.11	8.52	3.69	0.40	1.73
6383892436469819008	–	-129193.33	47.69	27.30	0.09	0.99	9.18
6729270234418615552	CD-38 13129	-129202.75	-108.51	27.57	0.38	0.97	6.07
5242632244811706496	TYC 9213-2091-1	-165717.38	-325.14	13.08	1.14	0.84	1.98
3155410389590889856	G 89-14	-168977.85	-176.82	12.65	0.50	0.92	0.85
32655224762711936	G4-36	-141767.94	114.54	20.51	0.09	0.99	14.55
3846427888295815552	HE0938+0114	-123889.65	-260.90	27.75	0.73	0.95	24.80
866863321051682176	BD+24 1676	-133448.07	-77.43	25.70	0.34	0.97	0.47
1289512635833404032	G166-47	-178769.02	-133.59	9.83	0.54	0.90	5.01
4761346872572913408	HIP 24316	-157275.95	-869.57	14.78	2.47	0.71	6.55
5181063205724188032	G75-56	-170575.00	-1466.88	9.94	5.06	0.33	1.65
1776289248313154688	BD+17 4708	-149027.24	-201.64	18.62	0.55	0.94	0.77
2658240166703766016	BD+02 4651	-172793.13	-626.12	11.27	1.65	0.75	1.61
4272653983123701120	G21-22	-163379.73	36.43	13.94	0.17	0.98	1.18
2910503176753011840	LTT2415.00	-121743.08	-2497.55	31.97	6.71	0.65	9.74
125750427611380480	G37-37	-95894.36	-410.31	51.67	1.25	0.95	28.61
29331710349509376	G05-19	-140895.94	-219.78	21.66	0.64	0.94	7.00
2905773322545989760	HIP 25659	-114045.58	-3228.30	39.49	7.99	0.66	2.48
5586241315104190848	HD59392	-178043.45	-640.99	10.32	1.68	0.72	0.47
5551565291043498496	CD-48 2445	-164908.62	-275.84	13.62	0.82	0.89	0.14
949652698331943552	G107-50	-167967.85	-777.61	12.60	2.00	0.73	0.45
5617037433203876224	W 0725-2351	-161949.71	-587.79	11.12	2.31	0.66	10.26
870628736060892800	G88-10	-178734.94	-650.69	8.68	2.38	0.57	5.33
1097488908634778496	G234-28	-161952.45	-428.06	13.14	1.22	0.83	6.85
6268770373590148224	HD 140283	-159638.76	-139.94	14.80	0.51	0.93	1.00
731253779217024640	HIP 52771	-173197.37	-547.17	10.80	1.68	0.73	4.68
791249665893533568	BD+51 1696	-167411.87	-64.93	12.75	0.33	0.95	1.09
2279933915356255232	BD+75 839	-172679.06	-37.69	11.70	0.31	0.95	1.09
2427069874188580480	HIP 3026	-177036.14	-80.12	10.72	0.39	0.93	1.37
5486881507314450816	HIP 34285	-146177.34	53.60	19.59	0.15	0.98	1.56
6859076107589173120	HIP 100568	-178122.94	-63.71	10.33	0.35	0.93	4.62
4468185319917050240	G 20-24	-169181.12	-209.53	12.24	0.70	0.89	4.55
4376174445988280576	BD +2 3375	-129172.93	141.57	27.43	0.25	0.98	0.52
588856788129452160	BD 9 2190	-127301.32	-1813.78	28.25	4.97	0.70	8.46
61382470003648896	G 5-40	-174809.98	-28.78	10.64	0.35	0.94	6.37
4715919175280799616	HIP 7459	-149799.68	-303.19	18.36	0.72	0.92	0.12
3643857920443831168	G64-37	-152525.63	-1058.08	15.01	3.08	0.66	8.64
5709390701922940416	HIP 42592	-168527.88	-608.18	12.16	1.61	0.77	3.31
5184824046591678848	LP 651-4	-172739.89	98.15	11.16	0.02	1.00	6.15
761871677268717952	BD 36 2165	-156655.26	-289.70	15.13	0.93	0.88	10.57
2722849325377392384	BD 7 4841	-176665.28	-44.94	10.87	0.24	0.96	0.23
16730924842529024	BD 11 468	-177010.67	-939.28	10.01	2.73	0.57	0.71
1458016709798909952	BD 34 2476	-142582.26	27.03	17.50	0.21	0.98	18.73
5806792348219626624	CD -71 1234	-122305.09	23.77	29.48	0.15	0.99	26.74
3699174968912810624	HE1208-0040	-174470.01	-652.29	10.57	1.86	0.70	1.15
4228176122142169600	G 24-25	-167077.60	-511.44	12.50	1.35	0.81	3.32
5133305707717726464	BD -17 484	-147101.71	-284.96	18.96	0.84	0.91	5.18

Table 3. Online Table: Enceladus Candidates from the GALAH survey with Li determinations. In the second column the flag Cannon from GALAH is reported. A flag Cannon = 0 means a reliable measurement (Buder et al. 2018)

Gaia source_id	f. c.	T_{eff}	log(g)	[Fe/H]	A(Li)
1732135056069825920	0	5033.32	2.64	-1.62	1.10
1753089552970858112	0	4509.55	0.85	-1.17	-0.06
2682935850698314240	0	5048.96	2.71	-1.77	1.29
2708796085010318592	0	5016.32	2.47	-0.86	1.34
2712879572412229504	0	4836.28	2.59	-0.48	1.11
2891158957586832384	0	4778.17	1.92	-1.25	1.20
2894294794812883072	0	5331.82	2.53	-1.02	1.42
2894411381703462400	0	5077.36	2.31	-1.08	1.32
2955975885301234176	0	5055.64	2.62	-0.93	1.43
2967759557578771712	0	4878.00	2.06	-0.63	0.57
2988442509461752704	0	5275.19	2.44	-0.84	1.27
3155073114396829696	0	5142.80	2.84	-1.79	1.34
3155410389590889856	0	5834.23	3.80	-1.32	2.32
3198867766340862464	0	5201.73	2.88	-1.30	1.44
3287575368035203456	0	4924.48	2.15	-1.51	1.06
3549336066900457856	0	4725.84	1.73	-0.91	0.67
4345499789558948608	0	4863.51	1.93	-1.63	1.13
4382559791045030912	0	5130.73	3.05	-1.75	1.27
4422595036636105984	0	5129.61	2.49	-1.05	1.40
4488499007696406784	0	4929.01	2.32	-0.87	1.13
4637675213429717376	0	4687.05	2.56	-0.50	0.72
4640304072716065280	0	4966.53	2.33	-0.92	1.39
4641720351067505024	0	5279.22	2.43	-1.13	1.57
4646028100186033152	0	4420.65	1.94	-0.34	-0.18
4685472457068177536	0	5119.64	2.77	-1.71	1.29
4693690589220392192	0	5581.52	3.64	-0.81	1.84
4699007101601586304	0	4739.82	1.78	-0.98	1.17
4701711045508666112	0	4904.03	2.08	-1.48	1.22
4705815178817583360	0	5087.22	2.25	-0.73	1.37
4725550450463451904	0	5857.36	3.79	-1.02	1.87
4775145228104639232	0	5221.97	3.06	-1.66	1.35
4881266547068247552	0	5060.26	2.79	-1.59	1.33
5225454471572336384	0	4656.60	1.46	-1.44	0.70
5226653836902677888	0	5119.06	2.30	-1.02	1.41
5242632244811706496	0	5985.94	3.90	-1.30	2.31
5374060481756321024	0	5056.90	2.68	-0.58	1.20
5384620324564238720	0	5125.24	2.36	-0.92	1.29
5389369703698845056	0	4625.94	1.85	-0.98	1.03
5395064211857452672	0	5097.59	3.16	-0.76	1.40
5401796104940236928	0	4988.28	2.35	-1.06	1.33
5458455798843435264	0	4855.07	2.12	-0.86	1.24
5459976109889190144	0	5929.12	4.03	-1.12	1.85
5470192432632884480	0	4982.57	2.72	-1.95	1.11
5668871503711755008	0	5156.47	2.87	-1.24	1.31
5673500722542380032	0	4905.31	2.03	-0.63	0.67
5676472530674105856	0	5090.21	2.47	-0.90	1.46
5728832958015766016	0	5063.25	2.58	-1.01	1.39
5729276503582050304	0	4707.00	1.70	-0.82	1.01
5750434405835685888	0	5834.30	3.84	-1.16	2.35
5752994756100253440	0	4969.32	2.39	-1.55	1.31
5781595596159463040	0	5935.60	3.92	-1.21	1.96
5791415819848472960	0	5122.25	2.72	-1.60	1.29
5807140176154682368	0	4773.03	1.79	-1.79	1.02
5816364872565566592	0	4823.02	1.97	-1.96	0.92
5818897872469627264	0	4961.09	1.79	-0.95	1.06
5946574193490564480	0	5981.59	3.83	-1.17	2.28
6002366471495563392	0	4969.72	2.34	-0.54	0.87
6002820050086770944	0	4458.54	0.98	-1.91	0.39
6014472781696679296	0	4837.48	1.97	-0.37	2.56

Table 4. Continue: Enceladus Candidates from the GALAH survey with Li determinations.

Gaia source_id	f. c.	T_{eff}	log(g)	[Fe/H]	A(Li)
6069724164405817856	0	4870.25	2.36	-0.65	0.66
6086864760409366656	0	5901.98	4.06	-0.90	2.32
6094877043381522688	0	5129.83	2.84	-1.19	1.48
6145484020253118208	0	5016.55	2.49	-1.37	1.30
6195538909150136960	0	5159.91	2.85	-1.30	1.52
6195538909150136960	0	5159.91	2.85	-1.30	1.52
6322264015162573952	0	5093.28	3.24	-0.55	1.17
6353051474611711232	0	5087.26	2.69	-1.65	1.27
6353984380164650624	0	4710.40	1.52	-1.27	1.00
6379689896869892480	0	4879.05	2.12	-1.12	1.26
6380579470496738688	0	5164.42	3.03	-1.68	1.41
6383892436469819008	0	5740.34	4.05	-1.23	2.19
6391140554558850432	0	5018.87	2.35	-1.27	1.46
6392042218516940416	0	5230.59	3.10	-1.80	1.33
6399437190128061824	0	4921.87	2.15	-1.35	1.35
6402012766053572096	0	5282.14	3.25	-1.53	1.48
6403691685950215808	0	4778.33	1.74	-1.56	1.20
6404161074334487808	0	4906.98	2.27	-1.35	1.26
6410480414335655680	0	4911.41	2.70	-0.67	0.84
6460648101957895040	0	4888.83	2.10	-1.35	1.37
6470581639759021056	0	4921.61	2.28	-1.26	1.38
6478310489244756224	0	4925.78	2.21	-1.15	1.39
6481444784579188352	0	5149.27	2.98	-1.84	1.36
6483276601013988864	0	5212.00	2.31	-0.88	1.12
6487462686594876544	0	4703.52	1.63	-0.92	0.60
6495347039663212800	0	4841.89	1.93	-1.31	1.15
6562694673781993472	0	5029.37	2.23	-0.98	1.23
6565548112614542592	0	5008.35	2.15	-1.24	1.33
6649405764224188416	0	5077.31	2.23	-0.62	1.13
6679323239394561792	0	5888.48	4.07	-1.16	2.23
6685311175422378368	0	5257.84	3.09	-1.61	1.43
6690424007572533120	0	4841.04	2.02	-1.17	0.65
6717997250935351680	0	4793.81	1.88	-1.38	1.15
6729270234418615552	0	5955.72	3.96	-1.24	2.01
6789958195324077824	0	4977.80	2.25	-1.25	1.12
6837496641407476224	0	5242.97	2.95	-1.13	1.52
6891710810994077568	0	4779.46	2.78	-0.39	0.64
3154778621377895936	1	5405.12	2.72	-1.06	1.64
3174650919659325952	1	5659.52	3.80	-1.43	1.97
3838992131675444480	1	5222.12	3.88	-1.26	1.29
4297160826005222656	1	6035.02	3.43	-1.04	2.00
4379282249962462336	1	5553.20	4.28	-1.21	1.54
4705330358613974144	1	5282.20	4.24	-1.23	1.25
4710644401389442048	1	5716.63	3.08	-1.00	1.65
4820909925710430976	1	5342.10	3.20	-1.79	1.43
5203339380025535104	1	5462.45	3.04	-1.06	1.79
5671614613424216064	1	5437.16	2.82	-1.09	1.64
5806792348219626624	1	6071.23	3.84	-1.27	2.26
5817597047142573952	1	5182.77	3.91	-1.49	1.44
6180667945665056768	1	5442.22	3.39	-1.61	1.68
6359046634778502144	1	5713.37	3.14	-1.20	2.02
6562024315286365568	1	5884.12	3.71	-1.20	2.12
6580611245819304320	1	5567.00	3.03	-1.18	1.56
6630376452061688704	1	5336.72	3.03	-0.98	1.74
6697722432614775040	1	5606.67	2.91	-0.92	1.66
5419728418033942528	2	4218.52	0.73	-0.78	-0.61
5947512381830659328	2	5043.14	2.89	-1.57	1.32
6682809550247700096	2	6026.64	3.94	-1.36	2.10
5607538065058737536	3	4711.13	0.89	-0.45	0.49
6694628127719929088	3	5017.92	1.69	-0.96	0.57
6198863767893020288	8	5198.20	3.02	-1.54	1.22
6095297464840155008	64	4843.43	2.15	-1.25	1.22
6381173172415485568	65	4834.19	3.92	-1.75	0.92